PIER M

(Received 18 March 2023, Accepted 19 May 2024, Scheduled 26 May 2024)

A New Method for Ship Detection in SAR Image Based on Finsler Information Geometry

Ke Wang, Meng Yang*, and Feng Cheng

Hangzhou Dianzi University, Hangzhou, China

ABSTRACT: This article introduces a novel ship detection method for Synthetic Aperture Radar (SAR) images that leverages the principles of Finsler information geometry. It employs the curvature features of a statistical manifold as a discriminative mechanism to diminish the impact of sea clutter and augment the contrast between a target and its background. The ambiguity of the local microstructure and statistical characteristics is partially resolved by using information theory to select metric definitions and curvature representation of non-European space. This method models sea clutter using the Gamma Distribution Function (GDF), transforming the detection challenge into an anomaly detection framework within the GDF space. This approach establishes a theoretical detection framework rooted in Finsler information geometry by integrating statistical modeling with Finsler geometry. It harnesses the Finsler characteristics of GDF space to extract the curvature feature representations for each GDF. Detection is achieved by applying one-class support vector machines (SVMs) to a matrix of curvature values derived from these representations. The detection algorithm unfolds in two primary phases. Initially, it utilizes a family of probability distributions to capture geometrical information. Subsequently, curved features are employed for target detection. Through rigorous experimentation with real datasets, the method demonstrates enhanced resilience to sea clutter and outperforms existing techniques for analyzing distribution families, validating its effectiveness and robustness.

1. INTRODUCTION

Synthetic Aperture Radar (SAR) is a versatile all-weather tool with high-resolution capabilities which uses active microwave sensors to measure electromagnetic fields scattered back from targets [1]. This technology has attracted significant attention for ship detection in marine remote sensing [2]. Research in this area primarily focuses on two methodologies: traditional machine learning techniques and advanced deep learning approaches. Despite its effectiveness in various fields, such as imaging [3], speech recognition [4], and natural language processing [5], deep learning requires extensive datasets [6]. Unfortunately, the scarcity of large high-quality datasets in certain areas leads to challenges such as overfitting, particularly when deep learning algorithms are applied. A notable issue is the requirement for local correlation in data samples; without this, the reliability of these models decreases, highlighting the need for improved detection standards and larger datasets to effectively leverage the full potential of deep learning.

Intensity threshold-based techniques are a cornerstone of SAR target detection, aimed at identifying pixels or clusters that stand out from their surroundings based on their intensity values [7]. These techniques rely on the premise that targets such as ships and background clutter exhibit statistically significant intensity differences. However, the dynamic and intricate nature of SAR environments often undermines these detectors because their statistical assumptions may not hold across varied and complex clutter scenarios [8]. To address these challenges, a wealth of research has been dedicated to overcoming the limitations inherent in these traditional adaptive-threshold detection methods. Recent advancements in exploiting the feature representation of SAR images have introduced innovative approaches aimed at enhancing the detection and analysis of targets, such as ships, amidst complex backgrounds. Highlighting a key innovation, [9] introduces a variance weighted information entropy method specifically crafted to quantify the local dissimilarity between a ship target and its adjacent clutter in SAR images. [10] achieves the extraction of robust image features suitable for detecting targets in SAR images, even under conditions of very low signal-to-noise ratio (SNR). Speckle clutter, which is a common issue in SAR imagery, complicates both the interpretation and practical application of these images. To address a critical challenge in SAR image analysis, [11] conducts a quantitative study on the impact of speckle clutter on ship detection performance. To uniquely utilize the intricate information present in SAR images, [12] introduces an innovative unsupervised ship detection method that leverages complex-signal kurtosis and multi-scale saliency. [13] proposes a ship detection method that capitalizes on SAR time series data, offering a dynamic approach to identifying ships over time. To address the challenges posed by the simplistic textures of targets against complex backgrounds, [14] introduces a technique based on probabilistic inference and data fusion. This method aims to significantly lower the false alarm rate and enhance the reliability of detection in an inherently challenging SAR imagery environment. [15] employs a Fisher vector encoding strategy to encapsulate multi-stage information of superpixels

* Corresponding author: Meng Yang (yangmeng@hdu.edu.cn).

within SAR images. [16] unveils a ship detection strategy tailored for high-resolution SAR images, which clusters spatially enhanced pixel descriptors. This approach leverages detailed information available in high-resolution data to improve detection accuracy. [17] introduces a superpixel-based coupled folded arm resonator (CFAR) approach for ship detection in SAR images. This method innovatively applies pixel intensity and spatial features, either in sequence or individually, within Euclidean space to discern targets from clutter. [18] ventures into the domain of information geometry with the introduction of a Riemannian metric. This advanced mathematical framework was designed to markedly enhance the contrast between ship targets and background clutter. [19] presents a ship detection method that utilizes Riemannian curvature features. This innovative approach aimed to exploit the microstructural characteristics of the parameter space and enhance the ability to discern ship targets amidst complex backgrounds. [20] introduces a comprehensive framework that integrates the Riemannian metric with a statistical optimization model. This combination not only boosts the target detection capabilities but also achieves notable resilience to clutter interference. In the rapidly evolving field of SAR image analysis, no single detection method has emerged as a universally accepted standard. Each introduced algorithm has unique strengths in specific scenarios, and each technique offers distinct advantages and faces particular limitations.

Finsler geometry, a field of growing importance in mathematics and physics, plays a pivotal role in the calculus of variations and has seen rapid development across diverse applications in physics and biology [21]. The use of a family of probability distributions is central to the application of Finsler geometry in practical contexts [22]. This study explores Finsler geometric structures, focusing on how these structures, based on probability distributions, can be applied to contemporary engineering problems. The key objective was to investigate the microstructure of the Finsler manifold with a specific application in enhancing ship detection in SAR imagery. The novelty of this work lies in the proposition of a viable method to harness Finsler geometry theory for the analysis of SAR images. This study lays out an actionable framework for an in-depth study and practical application of Finsler information geometry by employing Finsler geometric analysis. This interdisciplinary approach not only advances our understanding of Finsler geometry but also opens new avenues for its application in solving complex problems in SAR image analysis and beyond.

2. PROPOSED METHODS

In this section, the geometry of the family of Gamma distributions is studied. A class of Finsler metrics is defined by a vector field on a Riemannian space form. The model of Gamma random variable is embedded as a submanifold in Finsler manifold. In this way, the problem of detection is transformed into a curvature problem of space. The ambiguity of the local microstructure and statistical characteristics is partially resolved by using information theory to select metric definitions and curvature representation of non-European space.

2.1. S-Curvatures

With the development of mathematics, problems in a non-Euclidean space can be addressed. In other words, the structure focused on is a non-Euclidean metric. The essence is to study problems in a generalized space, where there is no higher-dimensional space for reference. The Riemannian property of a subspace in $\mathbb{R}^n$ is that it can be constructed using metrics based on the local Cartesian coordinates and intrinsic geometric properties, where there is no parametric representation for reference. The main idea of Riemannian geometry is to regard a surface as inherent in the universe itself, which is based on a quadratic differential form. Compared to the Riemannian geometry, the Finsler geometry metric has no restrictions on the quadratic form. That is, Finsler geometry has a richer geometric structure than Riemannian geometry [23]. In general, Finsler geometry provides specific theoretical bases, computing methods, and designing criteria for exploring the world of information science with high sensitivity, variability, and accuracy. The depth and scope of studies in the field of Finsler geometry must be improved. One of the main reasons for this is the complexity of calculations. Through continuous works of many researchers, their efforts have paid off, and the situation has also been gradually improved [24].

This study focuses on creating Finsler geometry structures of data and computing selected S-curvature indices from typical real SAR imagery. Furthermore, it is shown that feature representation — based on Finsler geometry — can improve target detection accuracy under inhomogeneous sea state conditions. One of the aims of this study is to provide useful insights into Finsler geometric methods in the analysis of image data. Although the application prospects of the results remain to be evaluated, we hope that these results will provide a reference to intelligence engineering.

Studies on Finsler geometry have focused on metrics, connections, geodesics, curvature, etc. In this section, we discuss some basic facts about Finsler spaces [24]. Let $\mathcal{M}$ be a manifold that is locally homeomorphic to a Euclidean space, such as a Euclidean space, sphere, manifold of probability distributions, manifold of positive measures, unitary matrices, and neural manifold. A Finsler metric F is defined as a function $F : T\mathcal{M} \to \mathbb{R}^n$ with the following properties: (1) Regularity property: F is $^\infty$ on $T\mathcal{M}/\{0\}$; (2) Positive homogeneity property: $F(x, \lambda y) = \lambda F(x, y)$ for all $\lambda > 0$; (3) Strong convexity property: The Hessian matrix $(g_{ij}) := ([2^{-1}F^2]_{y^i y^j})$ is positive-definite for all points of $T\mathcal{M}/\{0\}$.

In this case, $(\mathcal{M}, F)$ is called the Finsler manifold. Clearly, the restriction F_x defined on $T_x\mathcal{M}$ is a Minkowski norm. It follows from the homogeneity and convexity of F that $F(x, y) = \sqrt{g_{ij}y^i y^j}$. Take a local coordinate system (x^i, y^i) on the n-dimensional manifold and let $dV_F = \sigma_F(x)dx^1 \cdots dx^n$ denote the Busemann-Hausdorff F form of Finsler metric [24]; then,

$$\sigma_F(x) := \frac{Vol(B^n)}{Vol\{(y^i) \in \mathbb{R}^n \,|F(x, y^i(\partial/\partial x^i)|_x) < 1\}} \quad (1)$$

where Vol denotes the Euclidean volume, and $Vol(B^n)$ denotes the volume of the unit sphere in $\mathbb{R}^n$. Thus, $\sigma_F(x)$ is a measure function. Furthermore, if Finslerian volume is defined

in different ways, different theoretical results are obtained. In other words, one can choose a geometric statement depending on the needs of different problems.

The primary content of modern Finsler geometry includes exploring various object expressions on $\mathcal{M}$, such as connection transform under different coordinate changes. For $y \in T_x\mathcal{M}/\{0\}$, the distortion $\tau = \tau(x,y)$ is defined as the form $\tau(x,y) := 2^{-1}\ln\left[\det\left(g_{ij}(x,y)\right)\right] - \ln\sigma_F(x)$.

Let $c(t)$ be a geodesic with $(x,y) = (c(0),\dot{c}(0))$. The S-curvature is defined as [24] $S(x,y) := \frac{d}{dt}\left[\tau(c(t),\dot{c}(t))\right]\big|_{t=0}$ which is a measure of the distortion along the manifold geodesics. For Riemannian metrics, the S-curvature vanishes. The S-curvature S is isotropic if and only if a function $c = c(x)$ exists, which is defined on $\mathcal{M}$ and satisfies [25] $S(x,y) = c(n+1)F(x,y)$.

For general Finsler metrics, the Busemann-Hausdorff form dV_F may be expressed hardly by elementary functions. However, this can be done for Randers metrics. Randers space was first proposed to solve problems in general relativity. It has since been applied in many disciplines, such as mathematics, physics, biology, and informatics. A Randers metric is a special Finsler metric, which is usually represented as the form $F = \alpha + \beta$, where $\alpha = \sqrt{a_{ij}(x)y^iy^j}$ is a Riemann metric on $\mathcal{M}$, and $\beta = b_i(x)y^i$ is a 1-form on $\mathcal{M}$. $a_{ij}(x)$ and $b_i(x)$ satisfy $\sqrt{a^{ij}(x)b_i(x)b_j(x)} < 1$, where $(a^{ij}) = (a_{ij})^{-1}$.

According to Finsler geometric theory, a Randers metric $F = \alpha + \beta$ can be defined as a solution of the following equation on manifold $(\mathcal{M}, h)$ [25], $h(x, yF^{-1} - V_x) = 1$, where $h = \sqrt{h_{ij}(x)y^iy^j}$ is the Riemannian metric on $\mathcal{M}$, and V_x denotes a vector field of the vector field $V = V^i(x)\frac{\partial}{\partial x^i}$, which satisfy $h(x,-V_x) = \sqrt{h_{ij}V^iV^j} < 1$. Here, $F = \alpha+\beta$ can be expressed as the form $F = \lambda^{-1}\sqrt{\lambda h^2 + V_0^2} - \lambda^{-1}V_0$, where $h = \sqrt{h_{ij}(x)y^iy^j}$, $V_0 = h_{ij}V^iy^j$, and $\lambda = 1 - h(x,-V_x)$.

It has been proven that the S-curvature $S = c(n+1)F$ of the Randers metric F is isotropic if and only if the vector field V satisfies [25] $-4ch_{ij} = V_{i;j} + V_{j;i}$. Here, $V_{i;j}$ are the coefficients of the covariant derivative of vector field V with respect to h.

We assume that the 1-form $V^* := V_1dx^1 + V_2dx^2$ satisfies $-4ch_{ij} = V_{i;j} + V_{j;i}$. Let $\psi = \left\{\eta\left[\left(x^1\right)^2 + \left(x^2\right)^2\right] + 1\right\}V_1$ and $\phi = \left\{\eta\left[\left(x^1\right)^2 + \left(x^2\right)^2\right] + 1\right\}V_2$. Then, ψ and ϕ satisfy

$$\frac{\partial\psi}{\partial x^2} + \frac{\partial\phi}{\partial x^1} = 4\eta c x^1x^2\left\{\eta\left[\left(x^1\right)^2 + \left(x^2\right)^2\right] + 1\right\}^{-1} \quad (2)$$

$$\left[\eta\left(x^1\right)^2 + 1\right]\frac{\partial\psi}{\partial x^1} = \left[\eta\left(x^2\right)^2 + 1\right]\frac{\partial\phi}{\partial x^2} \quad (3)$$

$$\left[\eta\left(x^1\right)^2 + 1\right]\frac{\partial\psi}{\partial x^1} = -2c\frac{\left[\eta\left(x^1\right)^2 + 1\right]\left[\eta\left(x^2\right)^2 + 1\right]}{\eta\left[\left(x^1\right)^2 + \left(x^2\right)^2\right] + 1} \quad (4)$$

We then have the following equations:

$$\frac{\partial\psi}{\partial x^2} + \frac{\partial\phi}{\partial x^1}$$

$$= -\eta x^1x^2\left\{\frac{1}{\eta\left(x^2\right)^2 + 1}\frac{\partial\psi}{\partial x^1} + \frac{1}{\eta\left(x^1\right)^2 + 1}\frac{\partial\phi}{\partial x^2}\right\} \quad (5)$$

$$\left[\eta\left(x^2\right)^2 + 1\right]^{-1}\frac{\partial\psi}{\partial x^1} - \left[\eta\left(x^1\right)^2 + 1\right]^{-1}\frac{\partial\phi}{\partial x^2} = 0 \quad (6)$$

And

$$c = -\frac{1}{2}\left[\eta\left(x^1\right)^2 + \eta\left(x^2\right)^2 + 1\right]\left[\eta\left(x^2\right)^2 + 1\right]^{-1}\frac{\partial\psi}{\partial x^1} \quad (7)$$

If $\eta \approx 0$, we set $\eta = 0$. The Cauchy-Riemann equations are obtained $\frac{\partial\psi}{\partial x^2} + \frac{\partial\phi}{\partial x^1} = 0$ and $\frac{\partial\psi}{\partial x^1} - \frac{\partial\phi}{\partial x^2} = 0$. According to the theory of complex analysis, we analyze and work out the solutions to the equations. An exact analytical solution to these equations can be obtained.

$$\psi = C_1 + C_2x^1 - C_3x^2 + C_4\left[\left(x^1\right)^2 - \left(x^2\right)^2\right] - 2C_5x^1x^2 + C_6\left[\left(x^1\right)^3 - 3x^1\left(x^2\right)^2\right] - C_7\left[3\left(x^1\right)^2x^2 - \left(x^2\right)^3\right] \quad (8)$$

where C_i $(i = 1, \cdots, 7)$ are real constants.

2.2. Sectional Curvatures

Information geometry is a theoretical system developed based on differential geometry. It is primarily used in statistical analyses, control theory, neural networks, quantum mechanics, information theory, etc. This provides a way to understand probability statistics methods in geometric terms [26], which bridges the gap between pure mathematics and information science.

The choice of probability distribution model for background clutter in SAR image has been extensively studied. By analyzing the properties of SAR imagery, many concrete SAR statistical distributions have been developed over the past few decades. Among them, Gamma distribution is a commonly used statistical model for sea clutter in SAR imagery. The probability density function $f(z)$ of Gamma random variable Z is given by [27]

$$f(z) = \left(\frac{\kappa}{\gamma}\right)^{\kappa}\frac{z^{\kappa-1}}{\Gamma(\kappa)}\exp\left(-\frac{\kappa}{\gamma}z\right), \quad z > 0 \quad (9)$$

where γ and κ denote the scale and shape parameters, respectively, and Γ is the Gamma function. Set $\nu = \kappa\gamma^{-1}$, and we have the logarithm of $f(z)$, $\log f(z) = [(\kappa-1)\log z - \nu z] - [\log\Gamma(\kappa) - \kappa\log\nu]$. Thus, the Gamma Fisher matrix can be defined as:

$$h(x) = [h_{ij}] = \begin{pmatrix} \kappa\nu^{-2\rho} & -\nu^{-\rho} \\ -\nu^{-\rho} & \frac{d^2}{d\kappa^2}\ln\Gamma(\kappa) \end{pmatrix} \quad (10)$$

where $\rho = 25\gamma\sqrt{\Gamma(1+2\kappa^{-1}) - \Gamma^2(1+\kappa^{-1})}$ and $x = (x^1,x^2) = (\nu,\kappa)$. Hence, the set $\mathcal{M} = \{f(z)\}$ of the Gamma probability distribution family forms a two-dimensional manifold, where a probability density function $f(z)$ is a point of manifold $\mathcal{M}$, and $x = (x^1,x^2) = (\nu,\kappa)$ denotes a coordinate system. For convenience in writing, we

let $\partial_i = \frac{\partial}{\partial x^i}$ $(i = 1, 2)$. By a straightforward calculation, the sectional curvature η of the Riemannian manifolds $\mathcal{M}$ is given as follows:

$$\eta = \frac{1}{4}\nu^{-2}\left[\vartheta'(\kappa) + \kappa\vartheta''(\kappa)\right]\left[1 - \kappa\vartheta'(\kappa)\right]^{-1} \tag{11}$$

where $\vartheta(\kappa)$ denotes the digamma function.

2.3. One-Class SVM

One-class classification problem has been investigated in several fields for decades [28]. Among the most effective unsupervised approaches for one-class classification, one-class support vector machines (SVMs) have been successfully used in many applications. The concept of the one-class SVM algorithm is simple, that is, finding a hyperplane or circle the positive examples in the samples.

We adopted one-class SVM model [29] to learn the discriminative weights for the curvature features. The objective function of a one-class SVMs is described as a convex optimization problem.

$$\min_{w,\varsigma,\varepsilon} 2^{-1}\|w\|^2 - \varepsilon + \upsilon^{-1}N^{-1}\sum_{i=1}^{N}\varsigma_i \tag{12}$$

s.t

$$w^T G(S_i) \geq \varepsilon - \varsigma_i \tag{13}$$

where ε represents the soft margin which represents the hyperplane distance from the origin; G denotes the Gaussian kernel function; $\varsigma_i > 0$ is training errors; and $\upsilon \in (0, 1]$ denotes the control parameter which controls the trade-off between the training errors and the number of support vectors. The default value of this control parameter is set to 0.5.

2.4. Detection Algorithm

We focus on Randers metrics, which is the simplest non-Riemannian Finsler metric. Let

$$\alpha(x, y) = \frac{\sqrt{\left[1 - h_{ij}(x)V^iV^j\right]\left(h_{ij}(x)y^iy^j\right) + \left(\sum_i V^i(x)y^i\right)^2}}{1 - h_{ij}(x)V^iV^j} \tag{14}$$

and

$$\beta(x, y) = -\frac{\sum_i V^i(x)y^i}{1 - h_{ij}(x)V^iV^j} \tag{15}$$

where $y = (y^1, y^2) = \left(\nu(\kappa^2+\nu^2)^{-\frac{1}{2}}, \kappa(\kappa^2+\nu^2)^{-\frac{1}{2}}\right)$. Let $V = \sum_{i=1}^{2} V^i\partial x^i$ be defined by $V^1 := [\eta(x^1)^2 + 1]\psi + \eta x^1x^2\phi$ and $V^2 := [\eta(x^2)^2+1]\phi+\eta x^1x^2\psi$. For the Riemannian metric $\alpha(x, y)$ and the 1-form $\beta(x, y)$, $F = \alpha+\beta$ is a Randers metric. The isotropic S-curvature of F can be obtained as follows:

$$S(x, y) = c(x)F(x, y) \tag{16}$$

where, $c(x) = -\frac{1}{2}[\eta(x^1)^2 + \eta(x^2)^2 + 1][\eta(x^2)^2 + 1]^{-1}\frac{\partial\psi}{\partial x^1}$.

The implementation details are described as follows:

(1) A binary image (0-1 labels) is obtained using a CFAR detector based on Weibull distribution. Experimental parameters are set as follows: the size of target window is $h_1 \times h_1$; the size of guard window is $h_2 \times h_2$; the size of background window is $h_3 \times h_3$; and the false alarm rate (FAR) is P_{fa}. The parameters (μ, σ) of Weibull distributions are estimated by using the maximum likelihood estimation (MLE) method, and T denotes the detection threshold which is computed by $z(k, l) > \mu + \sigma T \Leftrightarrow$ *target pixel* and $T = \sqrt{6}\pi^{-1}\left[\log(-\log P_{fa}) + 0.576\right]$;

(2) A fixed-size sliding window ($h \times h$ pixels) is applied to the image for extracting patches of $h \times h$ around each pixel, which are used to estimate the parameters (ν, γ) of Gamma distribution model by the method of maximum likelihood. Let $x = (\nu, \kappa)$, $y = \left(\nu(\kappa^2+\nu^2)^{-\frac{1}{2}}, \kappa(\kappa^2+\nu^2)^{-\frac{1}{2}}\right)$, and $C_i = 1$ $(i = 1, \cdots, 7)$. The isotropic S-curvature value of each patch of $h \times h$ was individually estimated;

(3) After pre-screening pair-wise features, 0-1 label and isotropic S-curvature value, isotropic S-curvature values are divided into two categories: background and potential target. The one-class SVM classifier was learned and trained on background S-curvature values;

(4) The final detection is realized with respect to all such features (isotropic S-curvature values for all pixels of SAR image) by using the one-class SVM method, which, by its nature, finds targets that are statistically distinct from background clutters.

3. EXPERIMENTAL RESULTS AND ANALYSIS

3.1. Experimental Results

Space-borne SAR sensors are widely applied in the monitoring and analysis of oceans. New modes of operation have increased the flexibility of SAR sensors, and these sensors can now obtain extensive spatial-temporal resolutions and microwave images within the coverage range. Owing to the physics and geometry of the formation process, SAR has a peculiar nature and properties, such as speckle noise, discontinuous scenes, and moving objects. However, in practice, all of them can increase the difficulty of algorithm design and seriously affect the detection effect of the algorithm.

To test and evaluate detection performance of proposed method, two real SAR images are first used in experiments, which are shown in Figs. 1(a) and (b). Figs. 2(a) and (b) show the 3D plots of the SAR images. Sea clutter is the undesired radar echoes from fluctuant sea surface that is generally non-homogeneous and non-stationary. Speckle noise is an intrinsic property of SAR imagery. Many errors in ship detection are caused by mixed pixels and speckle noise in SAR images. The existence of speckle noise is particularly important and contributes to serious disturbances in the performance of target detection in SAR images.

Owing to the characteristics of coherent imaging of SAR, statistical modeling methods are often used for target detection. Many nonparametric, parametric, and semiparametric models for SAR imagery have been undertaken in the literatures. As nonparametric modeling usually involves more explanatory

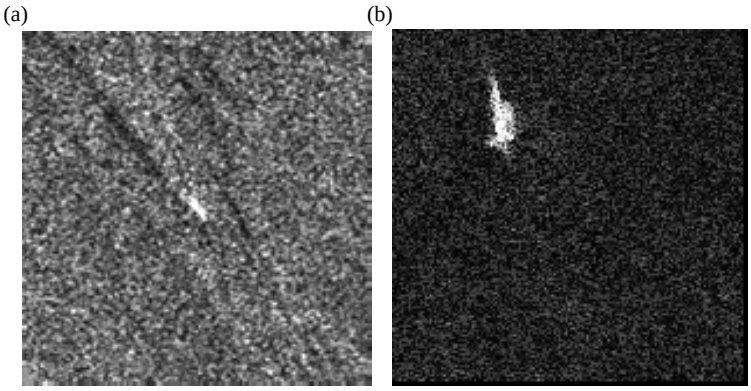

FIGURE 1. Original SAR images. (a) SAR image. (b) SAR image.

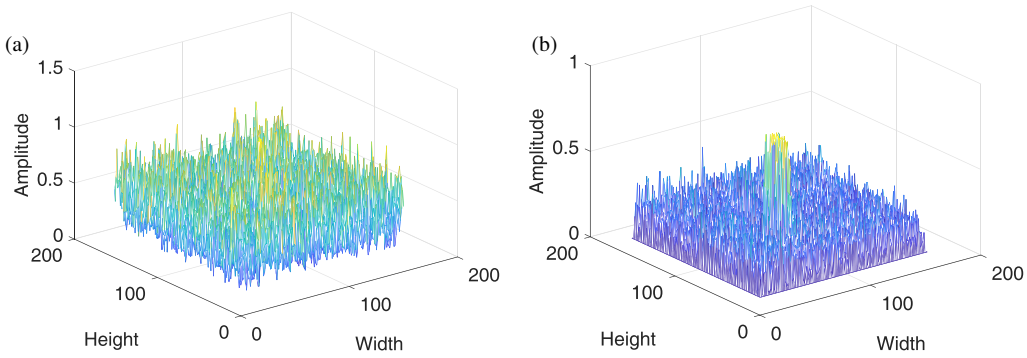

FIGURE 2. 3D plot of the images. (a) Fig. 1(a). (b) Fig. 1(b).

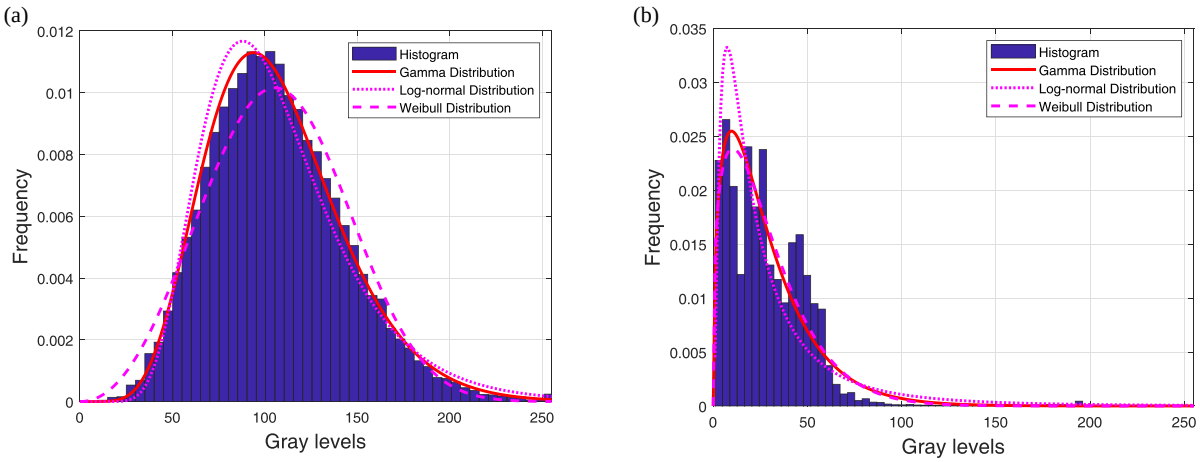

FIGURE 3. Histograms of two images. (a) Fig. 1(a). (b) Fig. 1(b).

variables, parametric and semiparametric models have been intensively studied. As shown in Figs. 3(a) and (b), SAR imagery has the characteristics of non-homogeneity and non-stationary. It is difficult to guarantee the accuracy of the designed models fitting to the real SAR image. It is expected that statistic-based detection performance can be improved by incorporating novel analysis techniques. This study presents a Finsler metric together with isotropic S-curvatures in a manifold of probability distributions. These geometric structures play important roles in wider areas of information sciences, such as signal processing, machine learning, automatic control, and even quantum information.

The first step of the algorithm is to adopt a pre-screening mechanism appropriate for target detection, which is used as pre-detection to obtain pre-screening pair-wise features, 0-1 label and isotropic S-curvature value. Among these methods, CFAR detectors are the most commonly used for ship detection in SAR images. This is achieved by estimating the threshold value based on the statistical characteristic of the pixels of the surrounding area. Because the pixel value above the threshold

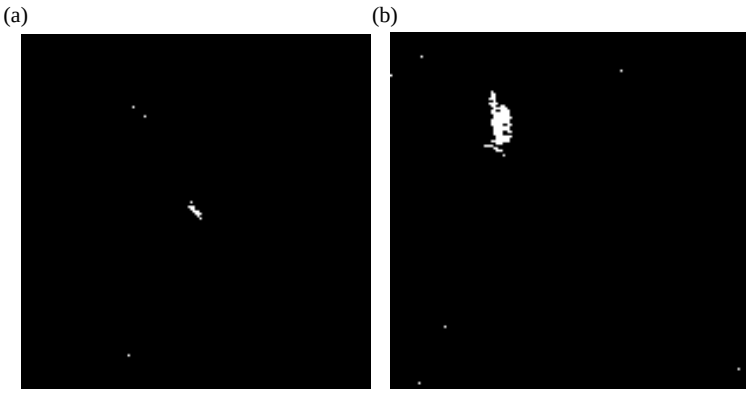

FIGURE 4. Binary classification and potential-target localization. (a) Fig. 1(a). (b) Fig. 1(b).

TABLE 1. Statistics characteristics for sectional curvatures of clutter.

Index	Maximum value	Minimum value	Expected value	Standard deviation	Median	Skewness
Fig. 1(a)	-3.37×10^{-41}	-5.31×10^{-17}	-5.30×10^{-21}	3.97×10^{-19}	-2.10×10^{-28}	-116.21
Fig. 1(b)	-6.78×10^{-38}	-2.88×10^{-11}	-9.87×10^{-15}	3.48×10^{-13}	-7.39×10^{-28}	-60.73

TABLE 2. Statistics characteristics for S curvatures of clutter.

Index	Maximum value	Minimum value	Expected value	Standard deviation	Median	Skewness
Fig. 1(a)	2.43×10^{-9}	-3.99×10^{-21}	5.02×10^{-12}	1.60×10^{-10}	1.91×10^{-14}	68.27
Fig. 1(b)	4.35×10^{-5}	-7.76×10^{-13}	7.17×10^{-7}	8.22×10^{-6}	2.61×10^{-10}	16.27

is declared as unusually bright, it may be a sample from the target. Clutter statistics in SAR images are typically analyzed using pixels in the background window around the pixel under test.

Without loss of generality, the commonly used adaptive threshold algorithm, namely CFAR detector under Weibull background, was adopted to obtain an initial coarse detection of the SAR image. As shown in Figs. 4(a) and (b), the pretreatment of SAR images is achieved using Weibull-based CFAR detection, and the integrity of the target areas is guaranteed. The experimental results demonstrate the effectiveness of CFAR for the initial coarse detection of SAR images.

The second step of the algorithm involves computing the isotropic S-curvatures for the one-class SVM. During the experiments, the two parameters (ν, γ) of the Gamma distribution were estimated using the MLE method, which can be implemented by extracting patches of $h \times h$ around each pixel under test. The isotropic S-curvature features of the target and background lying on the Finsler manifolds were used to enhance the performance of ship detection in SAR imagery. Subsequently, the calculation formulas were used to calculate the isotropic S-curvatures.

According to the theory of Finsler geometry on the statistical manifold, the S-curvature is constructed to measure the rate of change of distortion along geodesics, which is used for analyzing the variation of a family of Gamma probability distributions. Let $x = (\nu, \kappa)$, $y = (\nu(\kappa^2+\nu^2)^{-1}, \kappa(\kappa^2+\nu^2)^{-1})$, and $\nu = \kappa\gamma^{-1}$. As the set window is moved one pixel at a time across the entire image, the isotropic S-curvature value of the patch of $h \times h$ around each pixel of SAR image is calculated based on the estimated parameters (ν, γ). Table 1 lists the statistical characteristics of the sectional curvatures η of clutter. According to the preceding models, the isotropic S-curvature can be estimated using the presented formula, provided that η is small. Table 2 lists the statistics characteristics of the isotropic S-curvatures of clutter. Figs. 5(a) and (b) show the S-curvatures for each pixel with a high contrast between the target and background in SAR image. A comparison of the values in Table 2 and Fig. 5 indicates that the optimum features depend not only on the amplitude but also on the contrast with the background.

One of the aims of this study is to explore the invariant geometrical structure involved in statistical modeling using Finsler geometry. The S-curvature plays an important role in Finsler geometry, which interacts with the flag curvature in a very profound way. The flag curvature is a Riemannian quantity. This is a natural extension of the sectional curvature of Riemannian geometry. Many feature extraction techniques based on sectional curvature, which were developed for Riemannian space, can be carried over to Finsler space [24].

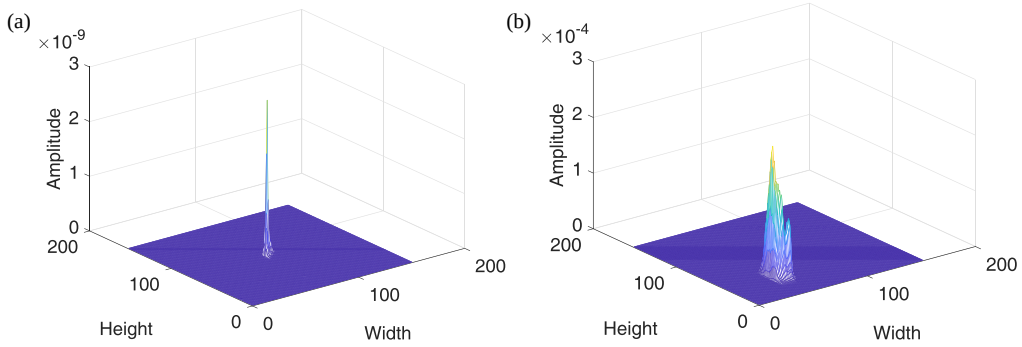

FIGURE 5. Isotropic S-curvature values. (a) Fig. 1(a). (b) Fig. 1(b).

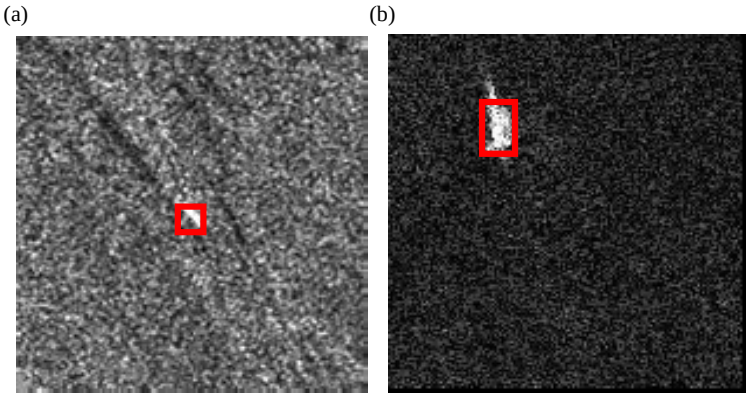

FIGURE 6. Final ship detection results. (a) Fig. 1(a). (b) Fig. 1(b).

TABLE 3. Experiment parameters used for ship detection.

Index	Modulation factor	Sliding window	FAR	Target window	Guard window	Background window
Fig. 1(a)	6	9×9	10^{-17}	9×9	15×15	25×25
Fig. 1(b)	4	15×15	10^{-17}	15×15	15×15	25×25

In the third step, according to the CFAR detection results (0-1 labels), the isotropic S-curvature values were divided into two categories: background and potential targets. Background S-curvature values were used to learn and train the one-class SVM model, which was used for anomaly detection in SAR images.

The final ship detection results were obtained using a trained one-class SVM classifier. As shown in Figs. 6(a) and (b), the proposed method provides a better detection performance for ship detection in SAR images.

The experiment parameters used for ship detection are shown in Table 3. The first parameter is the modulation factor ρ, which can be estimated according to the parameters (ν, γ) of the Gamma distribution model. The second parameter is the fixed-size sliding window ($h \times h$ pixels), which is used to extract patches of $h \times h$ around each pixel under testing and to estimate the parameters (ν, γ). The remaining parameters are provided for Weibull-based CFAR detector, which are used to obtain the initial coarse detection of the SAR image. In general, with several predefined parameters, the proposed method can be used to simultaneously detect targets of different sizes.

3.2. Experimental Analysis

For a quantitative assessment, we compared the detection results with the annotated dataset. The following measures allowed us to quantitatively assess the performance of several detection methods. $DR = TP(FN + TP)^{-1}$ and $FAR = FP(FP + TP)^{-1}$, where DR is the detection rate (DR); FAR denotes the false alarm rate (FAR); FN denotes the number of missing targets; TP denotes the number of detected targets; and FP denotes the false positive.

In the experiments, Gaofen-3 datasets [30] were used to evaluate the detection algorithms based on several performance measures. Gaofen-3 (GF-3) is China's first C-band multi-polarization SAR imaging satellite with a resolution of 1 m [31]. Its primary mission is to provide marine monitoring and ocean remote sensing. During the experiment, 1000 SAR images, in

TABLE 4. Comparison of performance for detection methods.

Index	DC-based CFAR [7]	Lognormal ρ-metric [8]	Geometric optimization [20]	Proposed method
DR	84.10%	84.23%	84.62%	84.97%
FAR	11.33%	4.22%	6.23%	4.13%

TABLE 5. Comparison of performance for detection methods.

Index	BTS-RCFAR [8]	SSMRI-based method [10]	Curvature-based saliency [19]	Proposed method
DR	93.33%	92.15%	90.79%	90.46%
FAR	10.24%	8.55%	4.01%	3.87%

which the land areas were masked out of the image being processed, were used to verify the performance of the detection methods via experiments. Morphological image processing is used to erase some false point-targets in binary images, which improves the quality of the binary detection image. In the experiment, the parameters were set as follows. The size of the sliding window is 15×15 pixels (used to estimate the parameters (ν, γ)); the size of the background window is 25×25 pixels, the size of the guard window is 15×15 pixels; the size of the target window is 15×15 pixels; and the FAR is $P_{fa} = 10^{-17}$. As shown in Table 4, the proposed model achieves a better FAR, which demonstrates its robustness and effectiveness.

In order to further verify the effectiveness of the proposed method, we perform experiments on Official-SSDD, which can be found in SAR ship detection dataset (SSDD): Official release and comprehensive data analysis. During the experiment, 1000 SAR images, in which the land areas were masked out of the image being processed, were used to verify the performance of the detection methods via experiments. From stationary and SNR of two aspects on clutter background, SSDD contains very high quality samples. The detection rate of this proposed algorithm is also very high.

CFAR-based detection algorithms are based on statistical background modeling. They are designed to search for bright pixel values that are also statistically unusual compared to the pixels in the surrounding area. The CFAR detector causes false alarms, even though the false alarm rate is especially low. Sea clutter is the backscatter from fluctuant sea surface and is generally non-homogeneous and non-stationary. Theoretical analyses and experiments indicate that the CFAR-based method has the feature of short computation time, high detection probability, high false alarming probability, and low anti-jamming performance [32]. For the Riemannian geometry method with various geometric structures, the detection performances are also different. Comparing the experimental results in Table 4 and Table 5, the proposed method, the curvature feature representation based on Finsler geometry, shows better anti-jamming performance.

The theoretical analysis and experimental results show that the proposed curvature framework using Finsler information geometry in the context of image analysis provides a natural and appropriate way to represent features from SAR imagery. The resulting information-geometry theory based on Finsler geometric structure provides a novel correspondence of statistic and geometry.

4. CONCLUSIONS

Compared with Riemannian geometry, Finsler geometry has no restrictions on the quadratic form, and Finsler geometry has a richer geometric structure than Riemannian geometry. Significant advances have been made in recent studies on Finsler geometry. The ideas and methods of Finsler geometry not only have an important effect on improving other mathematical branches but also possess potential applications in physics, control theory, informatics, etc.

Speckle noise is an intrinsic property of SAR imagery. The effects of speckle usually complicate SAR image detection and application. To overcome this limitation, this study proposes a curvature-based method for ship detection using SAR images. The main contribution of this work lies in the development of Finsler geometric feature. The sensitivity and efficiency of Finsler geometric feature were examined and demonstrated. These methods are suitable for the detection of ship targets in SAR images, but not for small target detection. Based on GaoFen-3 datasets, comparison studies validated the superiority of the curvature-based method for ship detection in SAR images.

Relying on modern differential geometry theory, this article offers an accessible entry point to Finsler information geometry for readers new to the area. One of the aims of this study is to synthesize Finsler geometric and statistical methods for target detection in SAR images. Theoretical analysis and experiments indicate that the Finsler geometry has shown great value and vitality. Future work will investigate how to use the S-curvature to explore highly variable, highly sensitive, and highly controllable functions in a non-Euclidean space, which can be applied to the deep learning models. It is a research field that uses modern mathematics theory and algorithms for deep neural network research. It is hoped that Finsler information geometry will build positive interactions between the methods and ideas of different groups in the future.

REFERENCES

[1] Shu, G., N. Wang, W. Wang, Y. Deng, Y. Zhang, H. Zhang, N. Li, and R. Wang, "A novel vortex synthetic aperture radar imaging system: Decreasing the pulse repetition frequency without increasing the antenna aperture," *IEEE Transactions on Geoscience and Remote Sensing*, Vol. 60, 5203014, 2021.

[2] Wang, X., G. Li, X.-P. Zhang, and Y. He, "Ship detection in SAR images via local contrast of Fisher vectors," *IEEE Transactions on Geoscience and Remote Sensing*, Vol. 58, No. 9, 6467–6479, 2020.

[3] Li, Y., X. Huang, and G. Zhao, "Joint local and global information learning with single apex frame detection for micro-expression recognition," *IEEE Transactions on Image Processing*, Vol. 30, 249–263, 2020.

[4] Shahamiri, S. R., "Speech vision: An end-to-end deep learning-based dysarthric automatic speech recognition system," *IEEE Transactions on Neural Systems and Rehabilitation Engineering*, Vol. 29, 852–861, 2021.

[5] Otter, D. W., J. R. Medina, and J. K. Kalita, "A survey of the usages of deep learning for natural language processing," *IEEE Transactions on Neural Networks and Learning Systems*, Vol. 32, No. 2, 604–624, 2021.

[6] Yang, R., G. Wang, Z. Pan, H. Lu, H. Zhang, and X. Jia, "A novel false alarm suppression method for CNN-based SAR ship detector," *IEEE Geoscience and Remote Sensing Letters*, Vol. 18, No. 8, 1401–1405, 2021.

[7] Wang, X., G. Li, X.-P. Zhang, and Y. He, "A fast CFAR algorithm based on density-censoring operation for ship detection in SAR images," *IEEE Signal Processing Letters*, Vol. 28, 1085–1089, 2021.

[8] Ai, J., Y. Mao, Q. Luo, M. Xing, K. Jiang, L. Jia, and X. Yang, "Robust CFAR ship detector based on bilateral-trimmed-statistics of complex ocean scenes in SAR imagery: A closed-form solution," *IEEE Transactions on Aerospace and Electronic Systems*, Vol. 57, No. 3, 1872–1890, 2021.

[9] Wang, X. and C. Chen, "Ship detection for complex background SAR images based on a multiscale variance weighted image entropy method," *IEEE Geoscience and Remote Sensing Letters*, Vol. 14, No. 2, 184–187, 2017.

[10] Xiong, G., F. Wang, W. Yu, and T.-K. Truong, "Spatial singularity-exponent-domain multiresolution imaging-based SAR ship target detection method," *IEEE Transactions on Geoscience and Remote Sensing*, Vol. 60, 5215212, 2022.

[11] Chen, S.-W., X.-C. Cui, X.-S. Wang, and S.-P. Xiao, "Speckle-free SAR image ship detection," *IEEE Transactions on Image Processing*, Vol. 30, 5969–5983, 2021.

[12] Wang, Z., R. Wang, X. Fu, and K. Xia, "Unsupervised ship detection for single-channel SAR images based on multiscale saliency and complex signal kurtosis," *IEEE Geoscience and Remote Sensing Letters*, Vol. 19, 4011305, 2021.

[13] Kahar, S., F. Hu, and F. Xu, "Ship detection in complex environment using SAR time series," *IEEE Journal of Selected Topics in Applied Earth Observations and Remote Sensing*, Vol. 15, 3552–3563, 2022.

[14] Zhang, C., C. Yang, K. Cheng, N. Guan, H. Dong, and B. Deng, "MSIF: Multisize inference fusion-based false alarm elimination for ship detection in large-scale SAR images," *IEEE Transactions on Geoscience and Remote Sensing*, Vol. 60, 5224811, 2022.

[15] Wang, X., G. Li, A. Plaza, and Y. He, "Ship detection in SAR images by aggregating densities of Fisher vectors: Extension to a global perspective," *IEEE Transactions on Geoscience and Remote Sensing*, Vol. 60, 5206613, 2021.

[16] Lang, H., Y. Xi, and X. Zhang, "Ship detection in high-resolution SAR images by clustering spatially enhanced pixel descriptor," *IEEE Transactions on Geoscience and Remote Sensing*, Vol. 57, No. 8, 5407–5423, 2019.

[17] Li, T., Z. Liu, R. Xie, and L. Ran, "An improved superpixel-level CFAR detection method for ship targets in high-resolution SAR images," *IEEE Journal of Selected Topics in Applied Earth Observations and Remote Sensing*, Vol. 11, No. 1, 184–194, 2018.

[18] Yang, M. and C. Guo, "Ship detection in SAR images based on lognormal ρ-metric," *IEEE Geoscience and Remote Sensing Letters*, Vol. 15, No. 9, 1372–1376, 2018.

[19] Yang, M., C. Guo, H. Zhong, and H. Yin, "A curvature-based saliency method for ship detection in SAR images," *IEEE Geoscience and Remote Sensing Letters*, Vol. 18, No. 9, 1590–1594, 2021.

[20] Yang, M., D. Pei, N. Ying, and C. Guo, "An information-geometric optimization method for ship detection in SAR images," *IEEE Geoscience and Remote Sensing Letters*, Vol. 19, 4005305, 2020.

[21] Chen, D., J. Zhu, X. Zhang, M. Shu, and L. D. Cohen, "Geodesic paths for image segmentation with implicit region-based homogeneity enhancement," *IEEE Transactions on Image Processing*, Vol. 30, 5138–5153, 2021.

[22] Amari, S.-I., *Information Geometry and Its Applications*, Springer, Tokyo, 2016.

[23] Bao, D., S.-S. Chern, and Z. Shen, *An Introduction to Riemann — Finsler Geometry*, Springer, New York, 2000.

[24] Shen, Y.-B. and Z. Shen, *Introduction to Modern Finsler Geometry*, Science Press, Beijing, 2013.

[25] Cheng, X. and Z. Shen, *Finsler Geometry — An Approach via Randers Spaces*, Science Press, Beijing, 2012.

[26] Ay, N., J. Jost, H. V. Le, and L. Schwachhofer, *Information Geometry*, Springer, Cham, 2017.

[27] Forbes, C., M. Evans, N. Hastings, and B. Peacock, *Statistical Distributions*, John Wiley & Sons, New York, 2011.

[28] Rasheed, W. and T. B. Tang, "Anomaly detection of moderate traumatic brain injury using auto-regularized multi-instance one-class SVM," *IEEE Transactions on Neural Systems and Rehabilitation Engineering*, Vol. 28, No. 1, 83–93, 2020.

[29] Hoang, T. M., N. M. Nguyen, and T. Q. Duong, "Detection of eavesdropping attack in UAV-aided wireless systems: Unsupervised learning with one-class SVM and k-means clustering," *IEEE Wireless Communications Letters*, Vol. 9, No. 2, 139–142, 2020.

[30] Sun, X., Z. Wang, Y. Sun, W. Diao, Y. Zhang, and K. Fu, "AIR-SARShip-1.0: High-resolution SAR ship detection dataset," *Journal of Radars*, Vol. 8, No. 6, 852–863, 2019.

[31] Hou, X., W. Ao, Q. Song, J. Lai, H. Wang, and F. Xu, "FUSAR-Ship: Building a high-resolution SAR-AIS matchup dataset of Gaofen-3 for ship detection and recognition," *Science China Information Sciences*, Vol. 63, 140303, 2020.

[32] Gao, G., *Characterization of SAR Clutter and Its Applications to Land and Ocean Observations*, Springer, Singapore, 2019.